View Online / Journal Homepage / Table of Contents for this issue
Dynamic Article Links

PCCP

Cite this: *Phys. Chem. Chem. Phys.*, 2011, **13**, 12798–12807

www.rsc.org/pccp

PAPER

Downloaded by Deutsches Zentrum fuer Luft- und Raumfahrt (DLR); Bibliotheks- und Informationswesen on 29 November 2011
Published on 20 June 2011 on http://pubs.rsc.org | doi:10.1039/C1CP20361D

Electrochemically induced oxygen spillover and diffusion on Pt(111): PEEM imaging and kinetic modelling

Eva Mutoro,†*[a] Christian Hellwig,[b] Bjoern Luerssen,[a] Sebastian Guenther,[c] Wolfgang G. Bessler[bd] and Jürgen Janek*[a]

Received 10th February 2011, Accepted 20th May 2011
DOI: 10.1039/c1cp20361d

Electrochemically induced oxygen spillover and diffusion in the Pt(O_2)|YSZ system is investigated in a combined experimental and theoretical study. The spreading of spillover oxygen is imaged by photoelectron emission microscopy (PEEM) on dense and epitaxial Pt(111) thin film electrodes prepared by pulsed laser deposition (PLD). Two different models are used to obtain surface diffusion coefficients from the experimental data, (i) an analytical solution of Fick's 2nd law of diffusion, and (ii) a numerical reaction-diffusion model that includes recombinative desorption of O_2 into the gas phase. The resulting diffusion coefficient has an activation energy of 50 kJ mol^{-1} and a preexponential factor of 0.129 cm^2 s^{-1} with an estimated uncertainty of ±20% for the activation energy and ±50% for the absolute value. The Fickian model slightly overpredicts diffusion coefficients due to the neglect of oxygen desorption. Experimental and theoretical results and limitations are discussed and compared to previous work.

Introduction

Electrochemically induced spillover and diffusion of oxygen on electrode surfaces plays an important role in solid state electrochemistry,[1] especially in the context of electrochemical promotion of catalysis (EPOC)[2] and electrocatalysis in solid oxide fuel cells (SOFCs).[1,3] In heterogeneous catalysis the concept of spillover indicates a migration of an adsorbed species from an active phase to a support or acceptor where some vital step in the reaction occurs.[4] In the field of EPOC, oxygen species originating from charge transfer are referred to as "(back)spillover" species. Often this term implies specific characteristics of the mobile oxygen—more strongly bound, (partly) negatively charged—differing from chemisorbed oxygen originating from the gas phase.[2] Despite its importance in EPOC, the nature and the properties of this species are not completely clarified yet,[5] and the detailed mechanism of EPOC is still under debate.[6–11] In the following, the term "spillover oxygen" refers to oxygen which is formed at the three-phase boundary (TPB) of the solid electrolyte (yttria stabilized zirconia, YSZ), the electrode (platinum, Pt) and the gas phase during anodic polarization and diffuses onto the electrode surface—without making any statement on its chemical and electronical nature.

In general, there are only a few methods available to investigate the spillover process *in situ*, that is, during electrochemical polarization. Indirect imaging has been demonstrated by inducing the consumption of a carbon film by spillover oxygen and visualising this reaction front using scanning photoelectron microscopy (SPEM).[12] This method offers chemical surface information on the micrometer scale, but the time resolution is not sufficient to image the relatively fast spillover process directly.[13] Photoelectron emission microscopy (PEEM) is a powerful method for investigating surface processes, such as surface diffusion[14] virtually in real time.[15] In the context of spillover oxygen, PEEM can distinguish between surface areas with and without adsorbed oxygen and provides high temporal and spatial resolution.[10,12,13,16,17]

This study aims at visualising the spreading of spillover oxygen—generated electrochemically at the TPB—by PEEM in order to understand in more detail the spillover and diffusion processes. We investigate the system Pt(O_2)|YSZ which is a model electrode system in solid state electrochemistry[1] as well as in EPOC studies.[2] Only the use of a (111)-oriented and covering Pt film model-type electrode with a well-defined TPB and sufficiently wide and flat Pt surface areas allows us to

[a] *Institute of Physical Chemistry, Justus-Liebig-University Giessen, Heinrich-Buff-Ring 58, 35392 Giessen, Germany. E-mail: juergen.janek@phys.chemie.uni-giessen.de; Fax: +49 (0) 641 9934509; Tel: +49 (0) 641 9934501*
[b] *German Aerospace Center (DLR), Institute of Technical Thermodynamics, Pfaffenwaldring 38-40, 70569 Stuttgart, Germany. E-mail: Wolfgang.Bessler@dlr.de*
[c] *Technische Universität München, Chemie Department, Physikalische Chemie mit Schwerpunkt Katalyse, Lichtenbergstr. 4, 85748 Garching, Germany. E-mail: Sebastian.guenther@tum.de; Tel: +49 (0) 89 289-1340*
[d] *Institute for Thermodynamics and Thermal Engineering, University Stuttgart, Pfaffenwaldring 6, 70550 Stuttgart, Germany*
† Current address: Electrochemical Energy Laboratory, Massachusetts Institute of Technology, 77 Massachusetts Avenue, MA, Cambridge 02139, USA. E-mail: emutoro@mit.edu.

This journal is © the Owner Societies 2011

View Online

Downloaded by Deutsches Zentrum fuer Luft- und Raumfahrt (DLR); Bibliotheks- und Informationswesen on 29 November 2011
Published on 20 June 2011 on http://pubs.rsc.org | doi:10.1039/C1CP20361D

image the spillover process and to extract kinetic data for the spillover species data analysis (which is not possible for highly porous films or paste electrodes). The mathematical modelling of the anodic spillover process as a diffusion phenomenon is possible, and we test two different theoretical models: an analytical solution of Fick's 2nd law of diffusion as a simplified approach ignoring desorption and a microkinetic reaction-diffusion model which takes all relevant microscopic processes into account. Both are used to describe the spillover phenomenon and to analyze it in terms of the spillover kinetics and result in data for the effective surface diffusion coefficient of the spillover species and its activation energy. The limitations of the approach are obvious but do not obstruct the approach: Firstly, the macroscopic character of the experiment does only result in averaged kinetic data. Secondly, in addition to the oxygen spillover process, other time-dependent processes, such as local morphology changes,[17,18] the formation of oxides at the electrode surface, or the Pt|YSZ interface can occur during electrochemical polarization and may then influence the spillover process. As these phenomena influence potentially the Pt/YSZ electrode kinetics, we include them in the discussion as far as necessary for the interpretation of the results.

Experimental

Sample preparation and characterization

Two different samples were investigated, a porous Pt electrode on polycrystalline YSZ (in the following referred to as "sample 1") and a dense, crystallographically oriented Pt film electrode on a YSZ(111) single crystal ("sample 2").

Electrolyte. Sample 1 consisted of polycrystalline YSZ (20 mm diameter, 1.5 mm thickness). The electrolyte of sample 2 was a (111)-oriented YSZ (9.5 mol% Y_2O_3) single crystal (CrysTec GmbH) polished on one side (average roughness < 0.5 nm) with the dimensions of $(10 \times 10 \times 1)$ mm^3. Potential impurity accumulation at the crystal surface (and thus, also at the electrolyte/electrode interface) after annealing was determined by time-of-flight secondary ion mass spectrometry (Tof-SIMS) and a XPEEM/XPS investigation of a comparable Pt film on YSZ after anodic polarization revealing silica impurities.[18]

Electrodes. The electrodes of sample 1 were prepared by applying and sintering ($T = 723$ K, $t = 2$ h and $T = 1123$ K, $t = 0.5$ h) Pt paste (Engelhard) twice. The working electrode (WE) covered about half of the electrolyte, while the counter (CE) and reference electrode (RE) were placed on the back. Note that we did not use a gas reference cell and thus the potential is not fixed ('pseudo reference electrode').

The WE of sample 2 was prepared by pulsed laser deposition (PLD, laser wave length 248 nm, repetition rate 6 Hz, pulse energy $\approx$ 450 mJ, temperature $T_{heater} = 973$ K, $T_{substrate} \approx$ 650 K, background gas Ar at 2 Pa, Ögussa Pt target 99.95% purity) as described in ref. 19 covering approximately half of the polished side of the electrolyte (macroscopic TPB length $l_{TPB} \approx 3.6$ cm). These essentially dense Pt films are (111)-oriented on the YSZ(111) substrates and contain only a few small defects. Detailed information (high resolution transmission electron microscopy (HRTEM), high resolution scanning electron microscopy (HRSEM), X-ray diffraction (XRD), energy-dispersive X-ray spectroscopy (EDXS), pole figures, cyclic voltammetry (CV), sample thickness) on the PLD film electrodes has been published previously,[19–21] including a study of their morphology changes during anodic polarization.[18] The CE and RE were prepared by sintered Pt paste (Ferro), resulting in a porous, polycrystalline network[18] comparable to the WE of sample 1. The CE was placed on the back of the electrolyte symmetrically to the WE, while the RE was located next to the WE (for electrode arrangement see the lower part of the experimental setup in Fig. 1).

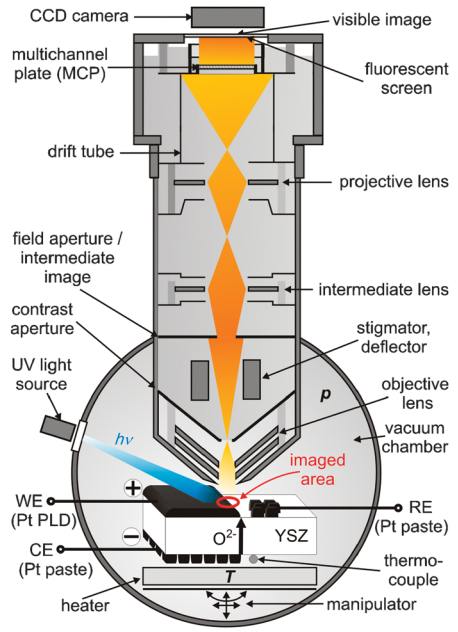

Fig. 1 Experimental setup: photoelectron emission microscope (PEEM) and geometry of sample 2 (not in scale). WE: working electrode; RE: reference electrode; CE: counter electrode; PLD: pulsed laser deposition; CCD: charge-coupled device.

Interface Pt|YSZ (sample 2). HRTEM images and EDXS investigations of these films showed an atomically sharp, semicoherent interface without any diffusion or segregation across the interface Pt(111)|YSZ(111) before electrochemical polarization.[19,20] In an XPEEM/XPS investigation we have observed Si contaminations at the interface and an accumulation at the TPB after anodic polarization in air[18] which indicates the possible presence and influence of impurities[22] in all studies.

Photoelectron emission microscope and experimental setup

Two different setups were used. Sample 1 was studied using a PEEM (self-construction, Institute of Physical Chemistry and Electrochemistry, University of Hannover) and a D_2 discharge lamp as an irradiation source (5 eV–6 eV). The measurement was carried out at $T = 670$ K and a base pressure of $p = 1 \times 10^{-9}$ mbar. For the investigation of sample 2 (Fig. 1) we used a Focus PEEM (Omicron NanoTechnology

Published on 20 June 2011 on http://pubs.rsc.org | doi:10.1039/C1CP20361D
Downloaded by Deutsches Zentrum fuer Luft- und Raumfahrt (DLR); Bibliotheks- und Informationswesen on 29 November 2011

GmbH) without an integral sample stage and a self-constructed sample holder on a separately mounted manipulator. This setup reduces the spatial resolution due to vibrations, but allows electrochemical characterization which is not possible with the integral sample stage. The sample temperature was measured with a thermocouple that was pressed on the back of the YSZ between the electrolyte and the sample holder. The UV irradiation source was a Hg discharge lamp ($I^{max} \approx 4.9$ eV). For imaging a cooled CCD camera (pco sensicam) was used. The sample heater and a thermal shield were placed behind the sample and measurements were carried out at three different temperatures in the order $T = 712$ K, 859 K, and 783 K. During the experiments the base pressure was $p = 1 \times 10^{-6}$ mbar.

The field of view of the microscope was determined on this sample by using a scratch on the Pt film with known dimensions. A small exposure time (0.1 s) of the camera was chosen in order to obtain a high time resolution which detrimentally affects the image noise and the spatial resolution.

Electrochemical polarization

For the electrochemical polarization we used a potentiostat/galvanostat (Jaissle IMP 83) and applied a polarization voltage $V_{WR} = 0.5$ V in potentiostatic mode.

Data analysis

General data treatment

The PEEM images of sample 2 were analyzed by dividing the electrode area into stripes parallel to the TPB with a width of several μm (see the first panel of Fig. 2b). The average photoemission intensity obtained from these areas was determined for different times t at each temperature. It was extracted by determining the grey level of the acquired PEEM images using IGOR Pro (macro).

The resulting data set consists of grey level values $G(x, t, T)$, where x denotes the distance from the TPB, t the time after electrode polarization, and T the substrate temperature. Due to the contrast mechanism in PEEM using low energy photon excitation, a high grey level G is obtained if the local work function is low and the coverage θ of an electronegative adsorbate, such as oxygen, is low.

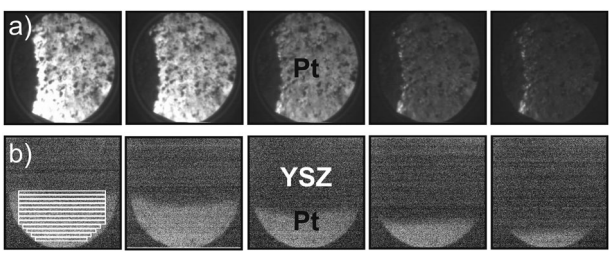

Fig. 2 Sequence of PEEM images during anodic polarization ($V_{WR} = 0.5$ V); (a) sample 1 (Pt paste electrode), field of view approximately 400 μm, interval $\Delta t = 1.2$ s, $T = 670$ K, (b) sample 2 (thin film Pt(111) electrode), field of view approximately 135 μm, interval $\Delta t = 0.4$ s, $T = 712$ K; in the first panel the positions where grey level intensities were extracted are shown as stripes.

Fickian diffusion model

As described previously,[12,13,17] a one-dimensional analytical solution of Fick's 2nd law of diffusion[23,24] was used for a first estimation of the diffusion coefficient D [cm^2 s^{-1}]:

$$\theta(x,t) = \frac{2q}{\Gamma N_A}\sqrt{\frac{t}{D}}\left[\frac{1}{\sqrt{\pi}}\exp\left(-\frac{x^2}{4Dt}\right) - \frac{x}{2\sqrt{Dt}}\mathrm{erfc}\frac{x}{2\sqrt{Dt}}\right]. \quad (1)$$

Here, $\theta(x, t)$ is the dimensionless local coverage of atomic oxygen on the electrode surface, q [atoms cm^{-1} s^{-1}] the rate of oxygen generated per unit length of TPB, t [s] the time, x [cm] the distance from the TPB, $\Gamma = 2.50 \times 10^{-9}$ mol cm^{-2} the density of Pt(111) adsorption sites, N_A Avogadro's constant, and thus the factor ΓN_A represents the number of adsorbed oxygen atoms of 1 monolayer ($\theta = 1$) on 1 cm^2 surface area.[25] Eqn (1) describes diffusion onto a semi-infinite surface with a constant influx q as a boundary condition. This simple model implies species conservation (no reaction or desorption) and a constant diffusion coefficient that does not depend on x or θ (*i.e.*, no interaction between diffusing species). Moreover, in the case of high rates q or large times t, the model can predict non-physical coverages above unity.

For fitting eqn (1) to experimental data, the photoemission intensity values G have to be converted and scaled in order to obtain coverages θ. We used the linear relation similar to the conversion procedure used for the low coverage regime for O on Pt(110)[26]

$$\theta(x, t) = aG(x, t) + b \quad (2)$$

where $a < 0$ because high θ results in low G. One might also perform the conversion using a relation of the PEEM intensity $I \approx (h\nu - \text{work function})^2$ as expected from so called Fowler plots.[27] Assuming a linear relationship between coverage and work function, the grey level can then be converted into the corresponding oxygen coverage. On the other hand, due to the rather small coverage changes of the obtained data set and the large errors intrinsically present in the analysis, the latter conversion was not performed as it changed the obtained coverage gradient curves only marginally.

The flux of the incoming oxygen atoms q can be expressed as a function of the electrical current at steady state I_{ss} [A],

$$q = \frac{I_{ss}N_A}{2Fl_{TPB}} \quad (3)$$

where l_{TPB} [cm] is the TPB length. Because the Fickian diffusion model is independent of absolute surface (pre)coverage, it does not allow us to determine the scaling offset b (eqn (2)); however, combining eqn (1)–(3) allows the quantification of the *change* of surface coverage $\Delta\theta$ upon polarization,

$$\Delta\theta(x,t) = \theta(x,t) - \theta(x,t=0) = a(G(x,t) - G(x,t=0))$$
$$= a\frac{I_{ss}}{l_{TPB}F\Gamma}\sqrt{\frac{t}{D}}\left[\frac{1}{\sqrt{\pi}}\exp\left(-\frac{x^2}{4Dt}\right) - \frac{x}{2\sqrt{Dt}}\mathrm{erfc}\frac{x}{2\sqrt{Dt}}\right] \quad (4)$$

Eqn (4) is fitted to the experimental data using D and a as free parameters.

 This journal is © the Owner Societies 2011

Published on 20 June 2011 on http://pubs.rsc.org | doi:10.1039/C1CP20361D
Downloaded by Deutsches Zentrum fuer Luft- und Raumfahrt (DLR); Bibliotheks- und Informationswesen on 29 November 2011

Numerical reaction-diffusion model

Obviously the assumptions leading to eqn (1) represent a strongly simplified description of the actual experiment: In fact, the diffusion zone has a finite length; the influx rate depends on the time (potentiostatic conditions) and the surface coverage at the TPB; the diffusion coefficient depends on the coverage; and the spillover oxygen atoms recombine and desorb as molecular oxygen.

In order to assess the influence of these processes on the evaluated diffusion coefficients, a numerical study of the coupled charge transfer, surface reaction, and surface diffusion processes was carried out. The modelling and simulation framework was adapted from previous work in the context of solid oxide fuel cells.[28–30] We assume that the PEEM samples can be represented in one dimension x perpendicular to the TPB line extending onto the Pt surface. The system of reaction–diffusion equations is given by

$$\frac{\partial\theta}{\partial t} = \frac{1}{\Gamma}\sum_m \nu_{i,m}\left(k_{\mathrm{f},m}\prod_{j\in \mathrm{R}_{\mathrm{f},m}} c_j^{\nu'_j} - k_{\mathrm{r},m}\prod_{j\in \mathrm{R}_{\mathrm{r},m}} c_j^{\nu''_j}\right) + \frac{\partial}{\partial x}\left(D_i^{\mathrm{surf}}\theta_{\square}\frac{\partial\theta}{\partial x}\right) \quad (5)$$

describing the change of surface coverage θ of atomic oxygen on Pt with time; see ref. 29 for a definition of all symbols and their units. The fraction of free surface sites is given by $\theta_{\square}$. The two terms on the right-hand side of eqn (5) are sources due to chemical reactions (adsorption, desorption, charge transfer) and surface diffusion, respectively. As a vacant site is required for an atomic jump to take place,[31,32] the diffusive flux is assumed to linearly depend on the fraction of free surface sites. Both, reaction rate constants k and diffusion coefficients D, are assumed to be thermally activated according to an Arrhenius behaviour,

$$D = D^0\exp(-E^{\mathrm{act}}/RT), \quad (6)$$

where D^0 is the preexponential factor, E^{act} the activation energy, and R the ideal gas constant. Diffusion of oxygen ions in the YSZ bulk is assumed to be fast and is not included in the model. We also assume that the YSZ surface does not provide a path for oxygen spillover and storage. To simulate the polarization behaviour, a counter electrode with fast oxygen exchange kinetics is assumed. The model requires the specification of thermodynamic, kinetic, and transport parameters of all species participating in the reaction system. These parameters are given in Table 1. Most parameters are taken from previous studies. For this study, we defined four free fit parameters: the preexponential factor and activation energy of the charge-transfer reaction as well as the preexponential factor and activation energy of the O_{Pt} surface diffusion coefficient. The model allows us to predict the complete dynamic behaviour of surface coverages in dependence on spatial position, temperature, pressure, and applied voltage using one single set of parameters.

The conversion of the PEEM intensity into adsorbate coverages according to eqn (2) had to be performed for each performed experiment using a best fit procedure between experiment and simulation. This proved to be necessary as the obtained photoelectron yield of each single experiment strongly depended on the microscope alignment, the sample surface, the MCP settings, and the adjustment of the illumination source.

Table 1 Species and reactions as well as thermodynamic, kinetic and transport data used in the numerical reaction-diffusion model. The reaction rate constants are calculated according to $k = k^0T^\beta\exp(-E^{\mathrm{act}}/RT)$. For the adsorption reaction, preexponential factors, activation energies, and temperature coefficients are converted from the sticking coefficient according to kinetic gas theory.[33] The surface site densities Γ of Pt and YSZ are 2.50×10^{-9} mol cm^{-2} [25] and 1.7×10^{-9} mol cm^{-2} [28], respectively. For a detailed description and derivation of the model see ref. 28 and 29

Species list and thermodynamic data at 780 K

Species	Molar enthalpy/kJ mol^{-1}	Molar entropy/J mol^{-1} K^{-1}	Comment
O_2	15.3	235	From NIST data base[34]
O_{Pt}	−99	52	Based on measured adsorption enthalpy of 213 kJ mol^{-1} [35] and estimated adsorption entropy[36]
$\square_{Pt}$	0	0	Free Pt surface site, reference values[33]
$O^{2-}{}_{YSZ}$	−236.4	0	Estimated[37]
$\square_{YSZ}$	0	0	Free YSZ surface site, reference values[33]

Reaction mechanism and kinetic data

Reaction	Preexp. factor k_{f}^0	Activation energy $E_{\mathrm{f}}^{\mathrm{act}}$	Sticking coefficient	Comment
$O^{2-}{}_{YSZ} + \square_{Pt} \rightleftharpoons O_{Pt} + \square_{YSZ} + 2e^-$	2.54×10^{-2} mol m^{-1} s^{-1}	197 kJ mol^{-1}		Charge transfer and spillover,[33] symmetry factor $\alpha = 0.5$; fit parameters. The reverse rate coefficients follow from the thermodynamic data.[28]
$O_{Pt} + O_{Pt} \rightarrow O_2 + \square_{Pt} + \square_{Pt}$	3.7×10^{17} m^2 mol^{-1} s^{-1}	(213–60θ) kJ mol^{-1}		O_2 recombinative desorption with coverage-dependent desorption energy[35]
$O_2 + \square_{Pt} + \square_{Pt} \rightarrow O_{Pt} + O_{Pt}$			0.023	O_2 dissociative adsorption, given in the form of a measured sticking coefficient of 0.023[38]

Surface diffusion coefficient

Species	Preexp. factor D^0/cm^2 s^{-1}	Activation energy E^{act}/kJ mol^{-1}	Comment
O_{Pt}	1.29×10^{-1}	50	Fit parameters

View Online

Downloaded by Deutsches Zentrum fuer Luft- und Raumfahrt (DLR); Bibliotheks- und Informationswesen on 29 November 2011
Published on 20 June 2011 on http://pubs.rsc.org | doi:10.1039/C1CP20361D

Results and discussion

Experimental results

The PEEM image of the polycrystalline Pt electrode (sample 1) darkened nearly homogeneously after applying the potential (V_{WR} = 0.5 V) as shown in a sequence of images in Fig. 2a. Three polarization experiments (V_{WR} = 0.5 V) at different temperatures (T = 711 K, 859 K, 783 K) were carried out on the dense Pt film electrode (sample 2). The resulting steady-state currents, that were reached shortly after applying the voltage, are listed in Table 2. The PEEM image darkened in a front spreading out from the TPB (Fig. 2b). The data resulting from the image analysis are shown as two-dimensional plots below (*cf.* Fig. 4).

Results of the data analysis

Fickian diffusion model. It was not possible to obtain a good fit of eqn (4) to a 3-dimensional data set (G, x, t at constant temperature). Instead, data sets (G, t) were used as basis for the fit at a single distance (x = 55 μm). The results of this analysis are shown in Fig. 3. The temperature-individual diffusion coefficients as well as their Arrhenius behaviour according to eqn (6) are given in Table 3. An activation energy of 81 kJ mol^{-1} was determined. It should be noted that performing the analysis at a different distance x resulted in different values for D. For instance, at a distance of 27.5 μm a fit was only possible at the two lower temperatures resulting in $D^{711\,K} = 6 \times 10^{-5}$ cm^2 s^{-1} and $D^{783\,K} = 2.7 \times 10^{-4}$ cm^2 s^{-1} and an E^{act} of 96 kJ mol^{-1}. This behaviour will be discussed below.

In addition, we roughly estimated the coverage change $\Delta\theta$ due to electrochemical polarization by calculating the number

Table 2 Polarization experiments and steady state currents

Experiment no.	Temperature T/K	Applied voltage V_{WR}/V	Steady state current I_{ss}/A
1	711	0.5	5.0×10^{-7}
2	859	0.5	2.5×10^{-6}
3	783	0.5	1.0×10^{-6}

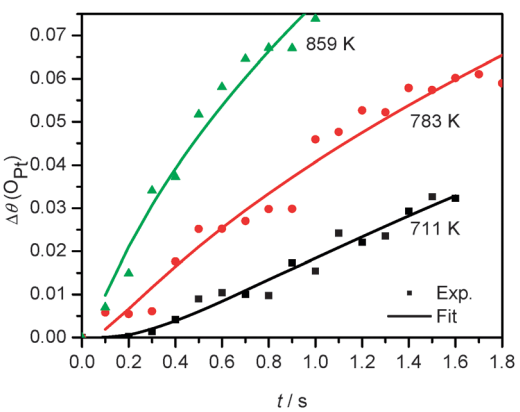

Fig. 3 Fickian diffusion model (eqn (4)): experimental and simulated change of surface coverage changes of atomic oxygen *vs.* time at a distance of 55 μm from the TPB at the three investigated temperatures.

Table 3 Fickian diffusion model for x = 55 μm: diffusion coefficients D at three different temperatures and resulting preexponential factor D^0 and activation energy E^{act}; changes of the oxygen surface coverages

T/K	711	783	859
D/cm^2 s^{-1}	2×10^{-5}	7×10^{-5}	2.1×10^{-4}
D^0/cm^2 s^{-1}	17		
E^{act}/kJ mol^{-1}	81		
$\Delta\theta$ (Fick's 2nd law, eqn (4))	0.033	0.061	0.074
$\Delta\theta$ (eqn (7))	0.090	0.127	0.159

of oxygen atoms diffusing on the surface within a certain time t using Faraday's law. For such an estimation the electrode area A_{spill} has to be determined which is covered by spillover oxygen at the time t after polarization. Using the PEEM data the time where the spillover front reached the distance of x = 55 μm away from the TPB was determined as 1.7 s at T = 711 K, 1.2 s at T = 783 K and 0.6 s at T = 859 K. Taking the total length of the TPB of the dense electrode and the distance x = 55 μm an area A_{spill} of 0.0195 cm^2 is obtained.

Under the simplified assumptions that all oxygen generated at the TPB is adsorbed homogeneously (no desorption, reaction, or consumption of oxygen due to an interfacial oxide, bubble formation, or reaction with CO, *i.e.* no coverage gradient perpendicular to the TPB of the electrode), $\Delta\theta$ can be estimated by

$$\Delta\theta = \frac{I_{ss}t}{\Gamma 2FA_{spill}} \qquad (7)$$

leading to the values shown in the lower row of Table 3. This simplification should be a reasonable approximation for short times and small distances to the TBP (directly at the TPB a Pt oxide formation is more likely[39]).

Numerical reaction-diffusion model. The predictions of the reaction-diffusion model are compared to the experimental data in Fig. 4. This figure shows the time-dependent coverage of Pt-adsorbed oxygen atoms for five different distances from the TPB at the three investigated temperatures. The values at t = 0 s represent the calculated O_2 adsorption/desorption equilibrium coverages. The overall agreement between simulation and experiment is good, and the simulation can reproduce the experimental trends over the complete data set. However at high coverages, the experimental data show a saturation-like behaviour that is not reproduced by the simulation, because the dark count level of the multichannel plate used for converting the electron image into visible light was reached; this is discussed below.

The absolute surface coverages show a considerable dependence on temperature, which is stronger than the coverage increase due to spillover. Starting from equilibrium (t = 0), the coverage increases upon polarization (t > 0 s). After a few seconds, the coupling between spillover, diffusion, and recombinative O_2 desorption leads to a smooth coverage plateau that represents the dynamic steady-state.

The surface diffusion coefficient determined through fit of the reaction-diffusion model has an activation energy of 50 kJ mol^{-1} and a preexponential factor of 0.129 cm^2 s^{-1} (Table 1). This procedure results in diffusion coefficients of

 This journal is © the Owner Societies 2011

Downloaded by Deutsches Zentrum fuer Luft- und Raumfahrt (DLR); Bibliotheks- und Informationswesen on 29 November 2011
Published on 20 June 2011 on http://pubs.rsc.org | doi:10.1039/C1CP20361D

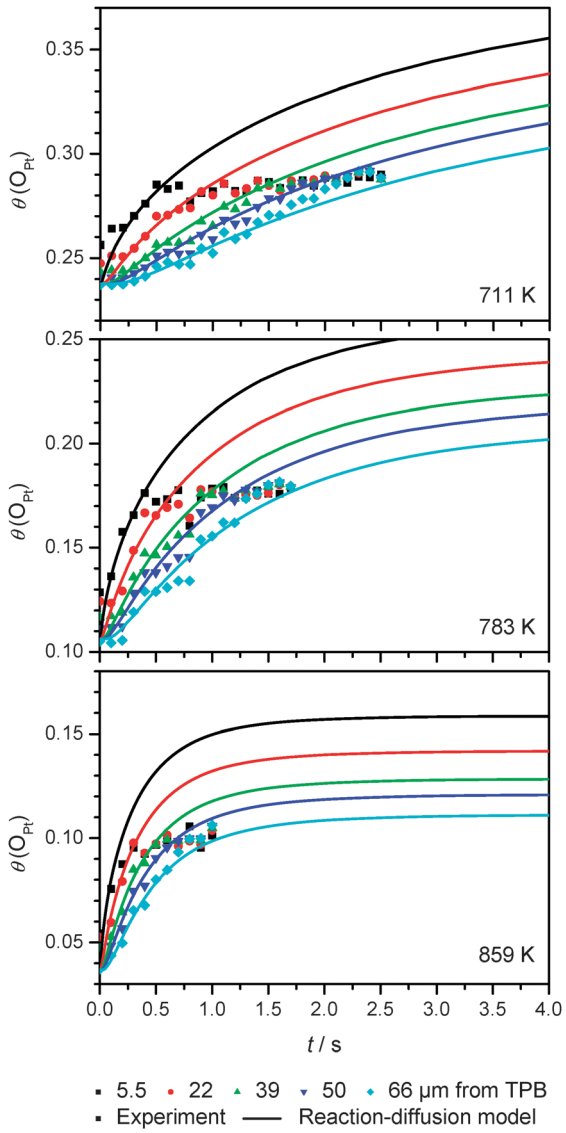

Fig. 4 Reaction-diffusion model (eqn (5)): experimental and simulated surface coverages of atomic oxygen *vs.* time after the application of voltage for different distances from the TPB at the three investigated temperatures. The coverages at $t = 0$ s represent the calculated O_2 adsorption/desorption equilibrium.

$D^{711\,K} = 2.7 \times 10^{-5}$ cm^2 s^{-1}, $D^{783\,K} = 6.0 \times 10^{-5}$ cm^2 s^{-1}, and $D^{859\,K} = 1.2 \times 10^{-4}$ cm^2 s^{-1}.

Fig. 5 shows the simulated time dependence of the electrical current (solid lines) and the steady-state experimental values (Table 2). The agreement between simulation and experiment is good. The simulations show an instantaneous onset of electrical current after voltage application, followed by a smooth decrease towards the steady-state value. The latter reflects the feedback of increasing surface coverage (Fig. 4) on the spillover reaction rate. Fig. 5 also includes the spatially integrated desorption rates of O_2 into the gas phase (broken lines). Desorption follows spillover somewhat delayed. In the steady state, the rates of oxygen entering the surface *via* spillover and leaving the surface *via* desorption are equal.

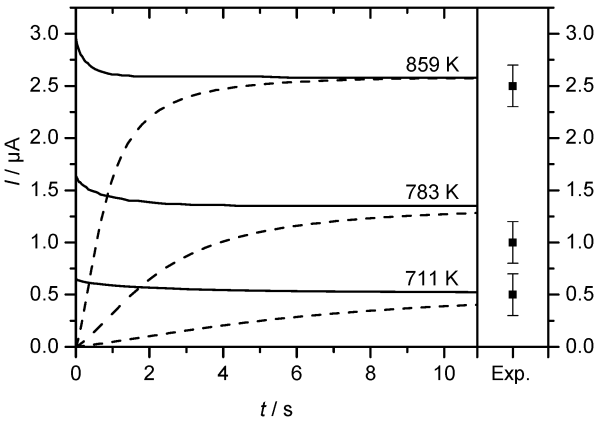

Fig. 5 Simulated electrical current (solid lines) *vs.* time after application of voltage at three different temperatures and steady-state experimental values (right panel). The spatially integrated desorption rate of O_2 is included as broken lines after conversion into units of current for quantitative comparison with electrical current (spillover rate).

Discussion

PEEM experiments

Adsorption of oxygen on a Pt surface changes the surface dipole and the surface potential χ, respectively, as shown in Fig. 6. An increased surface potential causes a higher work function Φ and, due to the work function change $\Delta\Phi$, the bright PEEM image turns dark. Thus even without direct chemical information, the change of the grey level in the UV-PEEM image of a Pt surface can be related to spillover oxygen—assuming there is no other process taking place changing the work function. However, using PEEM no statement on the chemical nature of this oxygen species can be given.

The nearly homogeneous darkening of the porous paste electrode (sample 1) can be explained by the large TPB length as a source for the diffusional spreading of oxygen on the geometrically complex Pt surface. The spatial resolution of PEEM is not sufficient to image a surface diffusion profile on this electrode. Spatial information could only be gained by

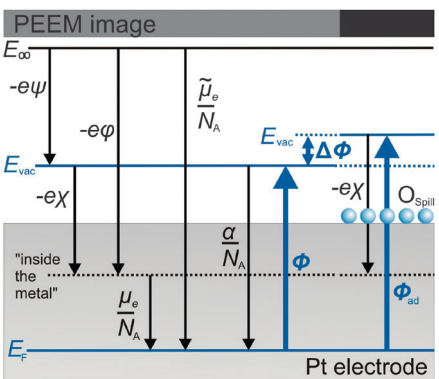

Fig. 6 Potentials (ψ = outer electric (Volta) potential, φ = inner electric (Galvani) potential, χ = surface potential, α = real potential, μ_e = chemical potential of an electron, $\tilde{\mu}_e$ = electrochemical potential of an electron), variation of the work function $\Delta\Phi$ ($= \Phi_{ad} - \Phi$) due to adsorption of oxygen (Φ_{ad}, O_{Spill}) and the corresponding grey level value of the PEEM image.

Published on 20 June 2011 on http://pubs.rsc.org | doi:10.1039/C1CP20361D
Downloaded by Deutsches Zentrum fuer Luft- und Raumfahrt (DLR); Bibliotheks- und Informationswesen on 29 November 2011

using the model-type electrode system with a reduced TPB length and a two-dimensional diffusion zone. In fact, the dense film model electrode used in this study (sample 2) provides defined boundary conditions for the analysis—for example, a linear TPB on a crystallographically oriented surface—reducing the complexity of the system. But even the model system bears some intrinsic disadvantages that have to be taken into account. However these drawbacks do not invalidate the approach, as discussed below:

(i) Morphology changes of the electrode may occur during anodic polarization[17,18] such as bubble formation due to the build-up of overpressure of oxygen underneath the electrode. Electrode detachment and hole formation by local dewetting of the metal electrode[40] can take place increasing the effective TPB significantly and changing the simplified geometry of the model electrode.

(ii) Recent *in situ* SEM experiments[41] revealed that an identically prepared TPB—or even different TPB locations on one sample—and the thin film Pt electrode close to the electrode edges can show a different behaviour regarding morphology changes, while in the inner electrode morphology changes occurred very uniformly. Potential reasons for this inhomogeneity are a slightly different film thickness gradient towards the electrode edges (and therefore a different dewetting behavior during annealing), different TPB microstructure, different adhesion (*e.g.* due to non-uniform impurity distribution at the electrode/electrolyte interface), or a blocking of TPB sites in a certain area due to inhomogeneously distributed impurities. This may also influence other processes starting at the TPB, such as oxygen spillover formation. Differently prepared TPBs, *e.g.* by shading during PLD film growth or by scratching the film, showed slightly different behaviour in PEEM during polarization.

(iii) The film thickness gradient at the electrode edges will lead to a negligible underestimation of the distance x to the TPB, and in combination with a low image intensity a small uncertainty in defining the starting point for diffusion. In addition, more surface steps—which may influence surface diffusion—will be present close to the TPB compared to inner electrode areas. Therefore, the determined diffusion coefficients represent averaged values for a surface with varying densities of steps and defects.

(iv) All samples have been assembled outside the UHV PEEM chamber. Impurities within the electrode system[18] may accumulate at the TPB and the electrode surface, thus influencing the experimentally determined diffusion coefficient. Contaminants which lower the work function, like alkali metals, might also contribute to the bright PEEM image before starting the polarization experiments. Even impurities in the solid electrolyte below the detection limit tend to accumulate at electrode interfaces where they may change the electrode kinetics.[18] However, we tried our best to reduce the influence of extrinsic contaminants and do not expect a major influence.

(v) As a consequence of points (i) to (iv) not on every sample a diffusion profile could be observed—also due to the experimentally sensitive assembly of the sample, frequently causing short circuits or contact problems. This might be in agreement with the observation that on some polycrystalline Pt films with a rougher topography and a few pores only parts of the surface darkened upon anodic polarization.[16] A sample having some porosity close to the TPB due to dewetting, for example, showed no clear spillover fronts.

In summary, it appears that the electrochemically induced spillover process is highly sensitive to electrode morphology, local microstructure, and impurities. As in heterogeneous catalysis, the "materials gap" and "pressure gap" have to be taken into account in using the present results for the interpretation of EPOC effects or Pt electrode kinetics in (μ-)SOFCs. Recent electrocatalytic experiments of comparable dense Pt PLD film electrodes on YSZ showed EPOC—although less pronounced than in the case of porous sintered paste electrodes.[42] Knowing that these model-type thin film electrodes show an EPOC effect, it remains as a future task to overcome the "pressure gap" and to apply high pressure spectroscopy/microscopy in order to obtain further insight. Our PEEM set-up does not allow measurements at ambient pressure.

Experiments and simulations show a different characteristic behaviour towards high coverages (Fig. 4). The experiments exhibit an abrupt saturation, that is, the grey level values change with time until they abruptly run into a constant value. The simulations show a smooth plateau, that is, the coverages increase with time and smoothly run into a constant value. This value depends on the distance from the TPB. The latter behaviour is expected from a reaction-diffusion system. We believe that the abrupt saturation behaviour is an artefact of the experimental setup that can be interpreted as follows: In order to emit photoelectrons from an oxygen-covered electrode, a photon energy of at least Φ_{ad} is required (*cf.* Fig. 6). If the UV light source cannot provide photons beyond this energy, the PEEM intensity will not decrease even with further increasing coverage. As the maximum energy of the used UV source (Osram HBO103W/2 lamp, $\sim$4.86 eV to $\sim$5.27 eV with an $I^{max} \approx 4.9$ eV) is close to the Pt work function (4.6 eV–5.9 eV),[27,43–45] this may well be the case in the present experiments. Depending on the exact work function of the investigated Pt film, only a part of the photons can be used, also explaining the observed low image intensity. Small amounts of (*e.g.* alkali) impurities lowering the work function of Pt may also contribute to the fact that the Pt film is visible.

Formation of Pt oxides

The formation of (impurity) oxides at the interface Pt/YSZ is likely,[18] but also the existence of a Pt surface oxide[46] has to be considered because of the high oxygen activities which can be electrochemically generated. Especially directly at the TPB a platinum oxide might form. Oxide formation would result in a reduced flux of oxygen available for spillover. However, there is no spectroscopic evidence for an interface or surface oxide formation under the experimental conditions so far; furthermore, if a thin oxide coverage existed (*e.g.*, in the ML range), this would not strongly influence our analysis. In addition, the Fickian analysis (Table 3), the estimation by Faraday's law (Table 3), and the reaction-diffusion model (Fig. 4) result in coverage changes—or coverages respectively—too low for an oxide formation ($\theta > 0.75$).[46] Thus, a surface oxide formation has not been included in the model analyses.

 This journal is © the Owner Societies 2011

Published on 20 June 2011 on http://pubs.rsc.org | doi:10.1039/C1CP20361D
Downloaded by Deutsches Zentrum fuer Luft- und Raumfahrt (DLR); Bibliotheks- und Informationswesen on 29 November 2011

Fickian diffusion model

Despite its simplicity, the Fickian diffusion model fits very well to the experimental data when considering one single distance x from the TPB (Fig. 3). However, it was observed that the resulting diffusion coefficients depend on x. The main reason for this is presumably the neglect of desorption of oxygen into the gas phase (Fig. 5, broken lines), which depends on absolute surface coverage and therefore on x. The desorption rate is higher close to the TPB, thus explaining the larger deviation between the analytical model and reaction-diffusion model at small x. Furthermore, the boundary condition of a constant flux of oxygen corresponds to a galvanostatic measurement and not to a potentiostatic one. However, as the steady state current I_{ss} was reached relatively fast (*cf.* Fig. 5), this probably induces a minor error only.

The lower coverage changes determined by the Fickian diffusion model compared to the ones estimated for an even distribution of all excorporated oxygen atoms on the Pt electrode surface (Table 3) also suggest an additional oxygen consuming process, like oxygen desorption.

In essence, the simple Fickian analysis should not be overrated. The neglect of desorption is a strong simplification, and the surprisingly good agreement with the experiment might be the combined effect of other simplifications (*e.g.* constant diffusion coefficient).

Numerical reaction-diffusion model

The detailed reaction-diffusion model allows the quantification of surface coverages based on a number of parameters that are either taken from the literature or used as free fit parameters in comparison with the experiments (Table 1). The achieved good agreement between experiment and simulation over the complete data set is a good indication for the validity of the model. Still, the resulting diffusion coefficients are subject to a number of uncertainties as discussed in the following.

(i) The adsorbed oxygen may not only be influenced by oxygen desorption into the gas phase, but potentially partly by reaction with CO present in the residual gas of the chamber. Both processes, desorption and reaction, reduce the amount of adsorbed oxygen.

(ii) *Sensitivity of parameter fit*. The experiment yields uncalibrated grey level values (our attempts to calibrate the grey level value using a reference with known work function were unsuccessful) that are scaled to the simulations. Grey level values of experiments at different temperatures are not related as the PEEM parameters had to be adjusted for refocussing the image after changing the temperature. Therefore, the validity of the model cannot be assessed based on the *absolute* coverages (which are not available from the present experimental setup), but only the *relative* behaviour of coverage with time and space, that is, the *shape* of the curves shown in Fig. 4.

For example, the activation energy of the diffusion coefficient needed to be varied by ± 10 kJ mol^{-1} in order to observe an unambiguous deviation between experiment and model after readjusting the scaling factors.

(iii) *Interdependence of other parameters*. The values used for the thermodynamics and kinetics of oxygen adsorption/desorption influence the steady-state and transient surface coverages and therefore the diffusion coefficient resulting from the fit. Uncertainties in the base data translate into uncertainties of the diffusion coefficients. For example, when neglecting the coverage dependence of the desorption energy (*cf.* Table 1), an activation energy of the diffusion coefficient of 41 kJ mol^{-1} was determined (instead of 50 kJ mol^{-1}).

Based on this discussion, we estimate the uncertainty of the obtained diffusion coefficient to be roughly $\pm 50\%$, including an uncertainty of the activation energy of $\pm 20\%$.

Comparison of models and previous studies

Fig. 7 summarises the results of the present study including a survey of published results from other studies. The Fickian diffusion model (Fig. 7c) results in slightly higher diffusion coefficients than the reaction-diffusion model (Fig. 7d). However, the deviation is significant only when the Fickian analysis is applied to the shorter distance x from the TPB. Here, the error induced by neglecting O_2 desorption is pronounced.

Oxygen diffusion on Pt—although not electrochemically induced and thus not fully comparable—has been studied using different experimental methods. Mostly the measurements were carried out at lower temperatures. We estimated the diffusion coefficients at higher temperatures according to eqn (6). The activation energy varies between 21 kJ mol^{-1} [47] for polycrystalline Pt and 41.5 kJ mol^{-1} [48] to 167.4 kJ mol^{-1} [26] for Pt single crystals. The preexponential factors differ strongly and vary over ten orders of magnitude (from 2.9×10^{3} [47] to 5×10^{-7} [48])—a fact which has already been discussed.[49]

Our own values for D are higher than most of the previous results from conventional diffusion experiments by about two orders of magnitude. We suggest that the difference may be caused by electrochemical polarization or by the uncertainty of the conversion of G to θ. Again, we have to emphasize that the obtained diffusion coefficient is an average for a surface with an unknown number of surface steps.

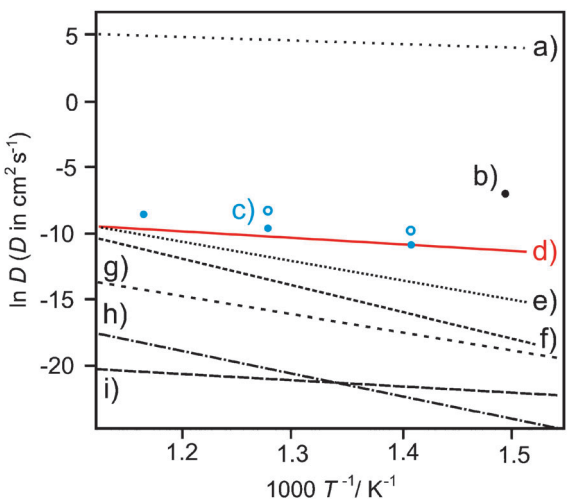

Fig. 7 Comparison of oxygen surface diffusion coefficients at higher temperatures. (a) Polycrystalline Pt, TDS,[47] (b) Pt(111), $V_{WR} = 0.2$ V, PEEM,[12,13] (c) this study, Fickian diffusion model, filled dots: $x = 55$ μm, empty dots: $x = 27.5$ μm, (d) this study, reaction-diffusion model, (e) Pt(100), $\theta < 0.2$, PEEM,[26] (f) Pt(100), $0.2 < \theta < 0.7$, PEEM,[26] (g) Pt(111), FEM,[50] (h) Pt(100), FEM,[47] and (i) Pt(111), STM.[48]

View Online

Downloaded by Deutsches Zentrum fuer Luft- und Raumfahrt (DLR); Bibliotheks- und Informationswesen on 29 November 2011
Published on 20 June 2011 on http://pubs.rsc.org | doi:10.1039/C1CP20361D

The different result of the previously published diffusion coefficient based on PEEM experiments ($D^{670\,K} = 9.2 \times 10^{-4}$ cm^2 s^{-1})[12,13] is most likely due to different experimental conditions: a polycrystalline Pt film electrode on a YSZ(100) crystal[24] was investigated at a smaller applied potential ($V_{WR} = 0.2$ V).[13] Furthermore, the analysis was only carried out at a single distance to the TPB and the maximum surface coverage θ_{max} was fixed to $\theta = 0.25$.

Recently, Imbihl *et al.* conducted PEEM measurements investigating electrochemical promotion of catalytic C_2H_4 oxidation with a polycrystalline Pt film having some pores on YSZ. They reported that a carbonaceaous adlayer poisoning the surface and their removal by spillover oxygen played an important role, and proposed to explain the non-Faradayicity as an ignition effect.[10,16] In agreement with our study, a homogeneous darkening of the PEEM image of Pt films with a smooth surface upon applying anodic potential was observed and explained by an increased oxygen coverage on the Pt surface. However, the sample preparation seemed crucial for observing spillover: on films with a rougher topography only parts of the surface darkened.[16] In addition to darkening of the PEEM image due to oxygen spillover, they observed the formation of bright spots in the PEEM image after several minutes upon applying a positive potential. The authors explain their appearance by the existence of SiO_x contaminations or by pores in the Pt film and a reduction of zirconia.[16] On a sample having some porosity close to the TPB and a number of small isolated Pt islands in front of the TPB, we also saw the formation of a brighter area in the PEEM image. The origin of this effect is unclear yet and will be subject of future work.

Conclusions

In the present study, we have demonstrated the use of PEEM as a well-suited method for the time-resolved imaging of spillover oxygen on metal electrodes in electrochemical experiments, allowing the evaluation of quantitative information on spillover kinetics. We also could show that only thin film model electrodes offer the necessary simplified diffusion geometry. Porous thick film electrodes, as obtained from sintered Pt pastes, are not suited for well-defined surface studies.

The theoretical modelling of the spillover kinetics was possible: two different models for data analysis were used in order to evaluate the diffusion coefficient of spillover oxygen on Pt(111) under reduced oxygen pressure. A reaction-diffusion model including recombinative O_2 desorption shows good agreement with the experimental data, not only in the case of the diffusion profiles but also for the current density across the TPB. The obtained diffusion coefficient has an activation energy of 50 kJ mol^{-1} and a preexponential factor of 1.29×10^{-1} cm^2 s^{-1}. The accuracy of the analysis was estimated to be ±50%, including an uncertainty of the activation energy of ±20%. The simplified analysis with a Fickian diffusion model yielded slightly higher diffusion coefficients, but can be regarded as reasonable first-order approximation.

The values for the diffusion coefficients and the activation energies should be considered with care, as they represent average values for transport across a surface with varying densities of steps and terraces. In addition, other channels for the annihilation of spillover oxygen than desorption (*e.g.* reaction with Pt, impurities or rest gas species) have been neglected, as these cannot be accounted quantitatively. These processes may shift the coverage scale, but the lateral coverage variation can still be analysed. Finally, morphological and microstructural changes of the Pt thin film electrodes upon polarization cannot be excluded, which may influence the local kinetics and the spillover diffusion profiles.

Thus, the two main conclusions are that (a) PEEM offers a unique method to image electrochemically driven surface diffusion, but that (b) the quantitative analysis is sensitive to details of the electrode microstructure and morphology, which may themselves change during the diffusion experiment. The reason for the partly different behavior of different TPB and electrode regions is not completely understood yet and will be part of future studies. We believe that further improvement in the preparation of chemically clean, epitaxial and microstructured thin film electrodes—in analogy to model surfaces in the study of heterogeneous catalysis—is the major obstacle for quantitative experiments with improved precision. The experimental approach itself has currently no alternative.

Acknowledgements

Financial support by the German Research Foundation (DFG) within the project Ja648/10-1 is acknowledged. WGB acknowledges funding by the Initiative and Networking Fund of the Helmholtz Association.

Notes and references

1 S. B. Adler, *Chem. Rev.*, 2004, **104**, 4791–4843.
2 *Electrochemical Activation of Catalysis*, ed. C. G. Vayenas, S. Bebelis, C. Pliangos, S. Brosda and D. Tsiplakides, Springer, 2002.
3 S. B. Adler and W. G. Bessler, *Elementary kinetic modeling of SOFC electrode reactions*, in *Handbook of Fuel Cells – Fundamentals, Technology and Applications*, ed. W. Vielstich, H. Yokokawa and H. A. Gasteiger, John Wiley & Sons, Chichester, UK, 2009, vol. 5, pp. 441–462.
4 *Handbook of Heterogeneous Catalysis*, ed. G. Ertl, H. Knözinger and J. Weitkamp, Wiley-VCH, 1997.
5 B. Luerssen, J. Janek and R. Imbihl, *Solid State Ionics*, 2001, **141**, 701–707.
6 V. A. Sobyanin and V. D. Belyaev, *React. Kinet. Catal. Lett.*, 1993, **51**, 373–382.
7 J. Janek, M. Rohnke, B. Luerssen and R. Imbihl, *Phys. Chem. Chem. Phys.*, 2000, **2**, 1935–1941.
8 A. Katsaounis, *J. Appl. Electrochem.*, 2010, **40**, 885–902.
9 Special Issue of *Catal. Today*, **146**, 265–386.
10 A. Toghan, L. M. Rosken and R. Imbihl, *Phys. Chem. Chem. Phys.*, 2010, **12**, 9811–9815.
11 R. Imbihl, *Prog. Surf. Sci.*, 2010, **85**, 241–278.
12 J. Janek, B. Luerssen, E. Mutoro, H. Fischer and S. Gunther, *Top. Catal.*, 2007, **44**, 399–407.
13 B. Luerssen, E. Mutoro, H. Fischer, S. Gunther, R. Imbihl and J. Janek, *Angew. Chem., Int. Ed.*, 2006, **45**, 1473–1476.
14 M. Snabl, M. Ondrejcek, V. Chab, W. Stenzel, H. Conrad and A. M. Bradshaw, *Surf. Sci.*, 1996, **352**, 546–551.
15 S. Gunther, B. Kaulich, L. Gregoratti and M. Kiskinova, *Prog. Surf. Sci.*, 2002, **70**, 187–260.
16 A. Toghan, L. M. Rosken and R. Imbihl, *ChemPhysChem*, 2010, **11**, 1452–1459.
17 E. Mutoro, B. Luerssen, S. Gunther and J. Janek, *Solid State Ionics*, 2008, **179**, 1214–1218.
18 E. Mutoro, S. Gunther, B. Luerssen, I. Valov and J. Janek, *Solid State Ionics*, 2008, **179**, 1835–1848.

 This journal is © the Owner Societies 2011

View Online

Downloaded by Deutsches Zentrum fuer Luft- und Raumfahrt (DLR); Bibliotheks- und Informationswesen on 29 November 2011
Published on 20 June 2011 on http://pubs.rsc.org | doi:10.1039/C1CP20361D

19 G. Beck, H. Fischer, E. Mutoro, V. Srot, K. Petrikowski, E. Tchernychova, M. Wuttig, M. Ruhle, B. Luerssen and J. Janek, *Solid State Ionics*, 2007, **178**, 327–337.
20 V. Srot, W. Watanabe, C. Scheu, P. A. van Aken, E. Mutoro and J. Janek, *EMC, Materials Science*, Springer-Verlag, Berlin Heidelberg, 2008, vol. 2, p. 369.
21 E. Mutoro, B. Luerssen, S. Gunther and J. Janek, *Solid State Ionics*, 2009, **180**, 1019–1033.
22 E. Mutoro, N. Baumann and J. Janek, *J. Phys. Chem. Lett*., 2010, **1**, 2322–2326.
23 *Growth and Diffusion Phenomena*, ed. R. B. Banks, Springer, Berlin, 1994.
24 S. Guenther, *Habilitation*, University of Hannover, 2003.
25 S. P. Devarajan, J. A. Hinojosa Jr. and J. F. Weaver, *Surf. Sci*., 2008, **602**, 3116–3124.
26 A. Von Oertzen, H. H. Rotermund and S. Nettesheim, *Surf. Sci*., 1994, **311**, 322–330.
27 H. H. Rotermund, S. Jakubith, S. Kubala, A. Von Oertzen and G. Ertl, *J. Electron Spectrosc. Relat. Phenom*., 1990, **52**, 811–819.
28 W. G. Bessler, S. Gewies and M. Vogler, *Electrochim. Acta*, 2007, **53**, 1782–1800.
29 M. Vogler, A. Bieberle-Hütter, L. J. Gauckler, J. Warnatz and W. G. Bessler, *J. Electrochem. Soc*., 2009, **156**, B663–B672.
30 W. G. Bessler, M. Vogler, H. Störmer, D. Gerthsen, A. Utz, A. Weber and E. Ivers-Tiffée, *Phys. Chem. Chem. Phys*., 2010, **12**, 13888–13903.
31 M. Tammaro and J. W. Evans, *J. Chem. Phys*., 1998, **108**, 7795–7806.
32 J. W. Evans, D. J. Liu and M. Tammaro, *Chaos*, 2002, **12**, 131–143.
33 R. J. Kee, M. E. Coltrin and P. Glarborg, *Chemically Reacting Flow. Theory and Practice*, John Wiley & Sons, 2003.
34 M. W. Chase, C. A. Davies, J. R. Downey, D. J. Frurip, R. A. McDonald and A. N. Syverud, *J. Phys. Chem. Ref. Data*, 1985, **Suppl 1**, 14.
35 J. Wintterlin, R. Schuster and G. Ertl, *Phys. Rev. Lett*., 1996, **77**, 123–126.
36 M. Tutuianu, O. Inderwildi, W. G. Bessler and J. Warnatz, *J. Phys. Chem. B*, 2006, **110**, 17484–17492.
37 W. G. Bessler, J. Warnatz and D. G. Goodwin, *Solid State Ionics*, 2007, **177**, 3371–3383.
38 S. Ljungström, B. Kasemo, A. Rosén, E. Wahnström and E. Fridell, *Surf. Sci*., 1989, **216**, 63–92.
39 H. Pöpke, E. Mutoro, C. Raiß, B. Luerßen, M. Amati, M. K. Abyaneh, L. Gregoratti and J. Janek, *Electrochim. Acta*, 2011, DOI: 10.1016/j.electacta.2011.04.057.
40 N. Baumann, E. Mutoro and J. Janek, *Solid State Ionics*, 2010, **181**, 7–15.
41 H. Poepke, E. Mutoro, B. Luerssen and J. Janek, *Solid State Ionics*, 2011, **189**, 56–62.
42 E. Mutoro, C. Koutsodontis, B. Luerssen, S. Brosda, C. G. Vayenas and J. Janek, *Appl. Catal. B – Environ*., 2010, **100**, 328–337.
43 H. Stöcker, *Taschenbuch der Physik*, Verlag Harri Deutscher, 2004.
44 J. Disdier, J. M. Herrmann and P. Pichat, *J. Chem. Soc., Faraday Trans. 1*, 1983, **79**, 651–660.
45 J. K. Schaeffer, L. R. C. Fonseca, S. B. Samavedam, Y. Liang, P. J. Tobin and B. E. White, *Appl. Phys. Lett*., 2004, **85**, 1826–1828.
46 S. P. Devarajan, J. A. Hinojosa and J. F. Weaver, *Surf. Sci*., 2008, **602**, 3116–3124.
47 M. U. Kislyuk, R. K. Nartikoev and Tretyakov, II, *Kinet. Catal*., 1982, **23**, 1013–1019.
48 J. Wintterlin, R. Schuster and G. Ertl, *Phys. Rev. Lett*., 1996, **77**, 123–126.
49 X. R. Wang, X. D. Xiao and Z. Y. Zhang, *Surf. Sci*., 2002, **512**, L361–L366.
50 R. Lewis and R. Gomer, *Surf. Sci*., 1968, **12**, 157–176.